Calculation of local mechanical properties of filled polymers

George J. Papakonstantopoulos,[1] Manolis Doxastakis,[1] Paul F. Nealey,[1] Jean-Louis Barrat,[2] and Juan J. de Pablo[1,*]
[1]*Department of Chemical and Biological Engineering, University of Wisconsin, Madison, Wisconsin 53706-1691, USA*
[2]*Université de Lyon; Université Lyon I; Laboratoire de Physique de la Matière Condensée et des Nanostructures; CNRS, UMR 5586, 69622 Villeurbanne, France*
(Received 11 November 2006; published 23 March 2007)

A study is presented on the effects of smooth nanoparticles on the structure and elastic moduli of a polymer matrix. Structural changes between the unfilled polymer matrix and the nanocomposite give rise to the formation of a glassy layer that surrounds the nanoparticles. Results for the effects of particle size and concentration on the local and overall mechanical properties of the polymer are consistent with experimental macroscopic observations. At the molecular level, it is found that dispersed, attractive nanoparticles alter the nonaffine displacement fields that arise in the polymer glass upon deformation, thereby rendering the nanocomposite glass less fragile.

DOI: 10.1103/PhysRevE.75.031803 PACS number(s): 61.41.+e, 62.20.Dc, 62.25.+g, 12.60.Rc

I. INTRODUCTION

Particulate fillers are used extensively by the polymer industry to alter the material properties of composite material. The addition of particles can lead to the strengthening of materials, thereby extending considerably their range of applicability. Supported by the ability to form arbitrary shapes and the advent of efficient processing techniques, polymer composites have found wide spread uses in everyday products. A significant amount of research has focused on the study of material properties in nanocomposite polymeric systems. In this context, changes of properties such as the glass transition temperature, mechanical constants, thermal expansion coefficients, gas permeability and solvent resistance are of fundamental interest and technological importance. Understanding the molecular mechanisms that lead to such modifications in the properties of nanocomposites is essential for design of materials having a desirable thermophysical behavior.

Polymer nanocomposites can exhibit an increase on the values of the mechanical properties [1–3] or a decrease [4,5], depending on the nature of nanoparticle-polymer specific interactions. Numerous experiments have been performed to investigate the mechanisms underlying such changes. One of the prevailing theories is the so-called interaction zone theory. Tsagaropoulos *et al.* [6] performed dynamical mechanical analysis (DMA) experiments for different nanocomposite systems. The stiffness of a viscoelastic material can be separated into two components, each of which describe two independent processes within the material namely, energy storage and energy dissipation. The ratio of dissipated to the reversibly exchanged work is known as "loss tangent" or tan δ. Tsagaropoulos *et al.* [6] have found two peaks in the tan δ versus temperature curves, suggesting the existence of two glass transition temperatures; the first was attributed to the polymer, and the second was attributed to the regions surrounding the particles. Using NMR experiments, Berriot *et al.* [7] concluded that, in rubber, silica fillers introduce supplementary topological constraints, thereby creating a layer of restricted chain mobility at the particle surface. The strength of the interaction was found to influence the degree of constraint. It was also found that the thickness of the aforementioned layer of "immobilized segments" at the particle surface was highly dependent on temperature.

Some of the parameters that affect the final properties of a composite are the particle size, the volume fraction and the extent of agglomeration. Experiments suggest that as the size of the particle decreases, the changes in mechanical properties become more pronounced [1,4,8]. "Large" microscale fillers reinforce polymers regardless of polymer-particle interaction. When the size of the particles decreases, this is no longer the case; depending on their size and their interaction, "nanoparticles" can increase or decrease the elastic moduli of a composite material [9–12]. Empirical relations proposed in the literature [9,13], and effective medium models [14–18], connect the filler volume fraction to the shear or Young's modulus and the viscosity. These correlations are, by construction, independent of particle size and are therefore unable to capture some of the physics that arise in nanocomposites. In effective medium approaches, the interfacial region is ignored and the matrix-nanoparticle bonding is assumed to be perfect. For large particle size fillers, these approaches explain a variety of experimentally observed phenomena, including the dependence of elastic moduli and viscosity on filler volume fraction. For small particles that dependence is no longer universal [19]. A complicating issue that arises in nanocomposites is the fact that particles often agglomerate [20], thereby changing the expected behavior and posing limits to the change in strength that can be achieved. Here we note that, recent studies [21] predict that elastic moduli can increase to a larger extent when particles agglomerate than when they are evenly dispersed.

Simulations provide a valuable tool for the study of nanocomposite systems. Although limited to the study of small volumes of material, they can offer useful insights into the spatial and structural arrangement of the particles in the polymer matrix. Unfortunately, simulations of the mechanical behavior of polymer nanocomposites have been scarce. Off-lattice simulations by Abrams and Kremer [22] of a

*Author to whom correspondence should be addressed. Electronic address: depablo@engr.wisc.edu

polymer melt interacting with a flat wall revealed a surface induced layering in the monomer density profile. These local density oscillations decrease as one moves away from the surface to the bulk polymer matrix. Simulation studies of polymers interacting with a wall by Aoyagi *et al.* and by Bitsanis and Hadziioannou [23,24] also showed a peak in the density near the wall that corresponds to an "adsorption" layer, and found that in going from weak to strong interactions between the wall and the polymer matrix the height of the peak increased considerably.

Vacatello [25] performed simulations of particles dispersed in a polymer matrix; he found that polymer sites in the immediate vicinity of the nanoparticle are arranged in densely packed and ordered shells. Polymer segments adhere to the particles and some chains are connected to different particles, thereby forming "bridges." Each chain visits the interface layer of several particles and each particle can be in contact with multiple chains. Even in the absence of strong attractive interactions between particles and polymer chains, Vacatello observed that the particles behave as physical crosslinks. These crosslinks do not immobilize the polymer chains, but they can reduce their diffusion rates considerably. That view was complemented by recent molecular dynamics simulations by Desai *et al.* [26], who found that chain diffusivity is enhanced (relative to that in the pure polymer) when polymer-particle interactions are repulsive, and is reduced when polymer-particle interactions are strongly attractive. These authors reported that chain diffusivity is spatially inhomogeneous, and adopts its pure-polymer value when the chain center of mass is about one radius of gyration R_g away from a particle's surface. Hooper *et al.* [27] have determined the effect of particle size on polymer-particle pair correlations to be small. The influence of particle size was calculated to be quite large for the surface excess though, and a transition was found from an entropic dewetting to enthalpic wetting interface.

Simulations and experiments have shown that nanoparticles can alter the dimensions of the chains vis-à-vis to those of the unfilled polymer. Previous work [28] has revealed that, in polymer solutions, the dimensions of a polymer chain change appreciably as it approaches the particle surface. At distances shorter than the mean size of the chain, an extension of the molecules takes place. It is also observed that the relative deformation is much smaller for longer chains. Changes in chain dimensions are confirmed by SANS experiments [29] on PDMS with PS nanoparticles; a decrease of the root-mean-square radius of gyration R_g is observed when the polymer chains are approximately the same size as the particles. A substantial increase of R_g is observed when the chains are much larger than them. These results support the view that filler particles cause an extension or contraction of the chains, thereby changing the stress required for elastic deformation.

Smith *et al.* [13] reported changes in the viscosity of a model polymer melt upon addition of nanoparticles. Results of simulations of polymers with attractive and neutral particles indicate that the viscosity increases above that of the unfilled polymer. For repulsive particles, the viscosity decreases. Brown *et al.* [30] also found that, for repulsive interactions between a particle and the polymer matrix, the bulk modulus of the composite, calculated from the density fluctuations, is lower than that of the pure polymer. Sharaf and Mark [31] used Monte Carlo rotational isomeric states simulations to define a reduced modulus and showed that it increases when chains are filled with spherical nanoparticles. They estimated a threefold modulus enhancement for their model.

Böhme and de Pablo [32] (for polymeric nanostructures) and Leonforte *et al.* [33] (for Lennard-Jones glasses) have analyzed the local displacement of individual molecules upon a homogeneous deformation. In both studies the local displacements were found to be highly nonaffine. The resulting nonaffine displacement exhibit a characteristic length below which the classical description of elasticity description breaks down; this characteristic length can be traced back to the "Boson peak" of the density of eigenstates [33].

Previously, we have verified the appearance of a glassy layer in the vicinity of a nanoparticle that is attractive to the polymer segments [34]. In this work we extend our investigation to the effect of particle size on the glassy layer thickness. Furthermore, we present a systematic study of the effects of particle size, concentration, surface area, and polymer chain length on the local mechanical properties of a simple nanocomposite glass model. Off-lattice Monte Carlo simulations of polymer matrices filled with spherical particles are employed. Mechanical properties are determined directly from the stress fluctuations and from small deformations of our samples. Our results are consistent with previous findings and augment the current understanding of nanocomposites by shedding light into the molecular origins of certain observed behaviors that occur upon addition of fillers in polymers. In particular, by examining the nonaffine local displacements of polymer segments that arise when the material is deformed, it is established that nanoparticles increase the mechanical homogeneity of the polymer glass and decrease its fragility.

II. METHODOLOGY

A. Simulations

In our simulations, the segments of the polymer molecules interact via a pairwise, 12-6 Lennard-Jones (L J) truncated potential energy function, shifted at the cutoff $r_c = 2.5\sigma$,

$$U_{nb}(r) = \begin{cases} 4\varepsilon\left[\left(\frac{\sigma}{r}\right)^{12} - \left(\frac{\sigma}{r}\right)^{6}\right] - U_{\mathrm{LJ}}(r_c), & r \leqslant r_c, \\ 0, & r > r_c, \end{cases} \quad (1)$$

where ε and σ are the Lennard-Jones parameters for energy and length, respectively, and r is the distance between two interaction sites. The bonding energy between two consecutive monomers in the same chain is given by

$$U_b(r) = \tfrac{1}{2}k(r-\sigma)^2, \quad (2)$$

with bond constant $k = 2 \times 10^3 \varepsilon/\sigma^2$. Nanoparticle-polymer segment interactions are described through a potential energy of the form [28]

$$U_{nb}^{f}(r) = \begin{cases} 4\varepsilon_f\left[\left(\frac{\sigma_f}{r-R_f}\right)^{12} - \left(\frac{\sigma_f}{r-R_f}\right)^{6}\right] - U_{\mathrm{LJ}}(r_c), & r - R_f \leqslant r_c \\ 0, & r - R_f > r_c, \end{cases} \tag{3}$$

where R_f is the radius of a nanoparticle and $\sigma_f=\sigma$. Two types of interactions are considered, strongly "attractive" ($\varepsilon_f=10\varepsilon$ and $r_c=2.5\sigma$) and "neutral" ($\varepsilon_f=\varepsilon$ and $r_c=2.5\sigma$). As can be seen from the form of the potential in Eq. (3), the interaction between a particle and a monomer is taken at a distance R_f (the radius of the filler) from the center of the particle. In that way the interactions are accounted for from the surface of the nanofiller.

The systems considered in this work consist of 450 chains of $N=32$ beads, or 120 chains of $N=120$ beads. Simulations are performed in the NPT ensemble. The pressure in all simulations is kept constant at $P=0.3\ \varepsilon/\sigma^3$. All quantities are reported in LJ units reduced with respect to the monomer σ and ϵ.

A Monte Carlo method is used to simulate the systems of interest to this work. Trial displacements include random monomer and nanoparticle translations. Reptation moves are also attempted, implemented within a configurational-bias scheme to increase performance [35]. While reptation can be effective in dilute systems of short chains, for intermediate to long chain molecules it is essential to resort to trial moves capable of rearranging inner segments of the polymer. To further enhance sampling, we also use internal rebridging trial moves [36], in which a number of consecutive monomers of a chain are selected and deleted. The deleted part of the chain is then reconstructed using configurational bias. We also implement double-bridging trial moves [37,38]; these moves consist of a simultaneous exchange of distinct parts of two neighboring chains, and are highly effective for configurational sampling of long chain molecules. Double bridging allows for effective equilibration of the systems considered in this work [37]. It is particularly important in nanoparticle-reinforced polymers, where sampling the correct structure and arrangement of long chain molecules around small nanoparticles can be particularly demanding.

All simulations in our study were performed for at least 9×10^4 Monte Carlo cycles, where a cycle consists of 5×10^4 trial moves. The maximum distance for the random displacement moves was chosen at each temperature so that an acceptance ratio of approximately 30% was achieved. Moving to lower temperatures and consequently higher densities, rebridging moves were performed with decreasingly fewer particles to maintain a reasonable acceptance probability. For the double bridging move the acceptance ratio is 0.005% if one segment is deleted and rebuilt (for proposed orientations for the configurational bias scheme at a temperature of $T=0.6$).

B. Formula for mechanical properties

The elastic moduli of solids can be calculated by measuring the thermal fluctuations of the internal stress; local mechanical properties can be determined by dividing the simulation cell into smaller cubes of length l [39]. In order to find the local elastic constants, a local stress must be defined. By performing a microscopic momentum balance flux balance on a cube m, the following expression for the local stress tensor can be derived:

$$\sigma_{ij}^{m} = \rho^m k_B T \delta_{ij} - \frac{1}{l^3}\sum_{a<b}\left(\frac{\partial U}{\partial r^{ab}}\right)\frac{r_i^{ab} r_j^{ab}}{r^{ab}}\frac{q^{ab}}{r^{ab}}, \tag{4}$$

where ρ^m is the number density of cube m, k_B is Boltzmann's constant, T is the temperature of the system, and δ_{ij} is the Kronecker delta. Subscripts denote Cartesian coordinates; U is the pairwise additive potential energy function and r^{ab} is the distance between two interaction sites a and b. If the vector joining a and b, r_i^{ab}, passes through cube m the fraction of the line segment that lies inside the cube defines the variable q^{ab}. If the vector does not pass through the cube then $q^{ab}=0$. Integration of σ_{ij}^m over the entire volume gives the internal stress tensor of the bulk system.

The local elastic modulus tensor, C_{ijkl}^m, is related to the internal stress fluctuations through the second derivative of the free energy with respect to the strain [39,40],

$$C_{ijkl}^{m} = C_{ijkl}^{Bm} - C_{ijkl}^{\mathrm{Sm}} + C_{ijkl}^{Km}, \tag{5}$$

where

$$C_{ijkl}^{Bm} = \frac{1}{l^3}\left\langle \sum_{\alpha<\beta}\left(\frac{\partial^2 U}{\partial r^{ab2}} - \frac{1}{r^{ab}}\frac{\partial U}{\partial r^{ab}}\right)\frac{r_i^{ab} r_j^{ab} r_k^{ab} r_l^{ab}}{(r^{ab})^2}\frac{q^{ab}}{r^{ab}}\right\rangle, \tag{6}$$

$$C_{ijkl}^{Sm} = \frac{V}{k_B T}[\langle \sigma_{ij}^m \sigma_{kl}\rangle - \langle \sigma_{ij}^m\rangle\langle\sigma_{kl}\rangle], \tag{7}$$

$$C_{ijkl}^{Km} = 2\langle\rho^m\rangle k_B T(\delta_{il}\delta_{jk} + \delta_{ik}\delta_{jl}), \tag{8}$$

and where V is the volume of the system. The brackets denote a canonical ensemble average; C_{ijkl}^{Bm} represents the instantaneous elastic modulus for any given configuration under a uniform, infinitesimally small strain (the so-called Born term). The contributions of internal particle motions (caused by the thermal fluctuations) to the elastic moduli are accounted by the stress-fluctuation term, C_{ijkl}^{Sm}. The contribution of the kinetic energy to the moduli is denoted by C_{ijkl}^{Km}.

C. Nonaffine displacement field

In this section we describe the technique used to calculate the nonaffine displacement field that arises when a material is deformed. The energy of a configuration is first minimized. A deformation is then imposed by rescaling all the atomic coordinates in an affine manner. The energy of this affinely deformed configuration is minimized again, keeping the simulation box shape and volume constant. This process yields particle or segmental displacements relative to the affinely deformed state. This analysis is performed on the pure polymer and nanocomposite systems of volume fraction $\phi\sim0.07$ and particle size $R_f=2\sigma$. The configurations used were created with two methods. One set of four configurations was obtained by gradual cooling of the system at con-

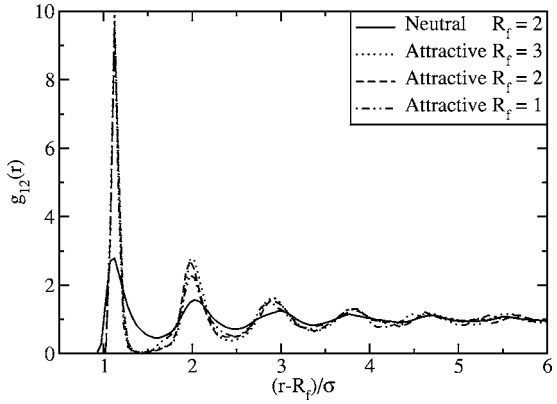

FIG. 1. Filler-monomer pair distribution function $g_{12}(r)$ for the various types of interactions considered in this work. All results are shown as a function of the distance $r-R_f$ from the surface of the nanoparticle at $T=0.6$, $P=0.3$, and $N=32$. The layers are well defined and the effect is more pronounced for attractive particles.

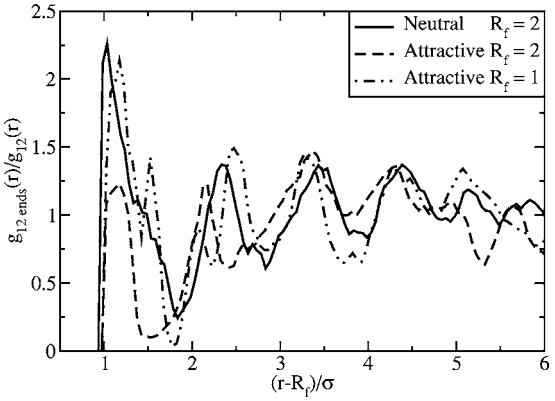

FIG. 2. Normalized filler-chain end pair distribution function $g_{12}^{\mathrm{end}}(r)/g_{12}(r)$ for both types of interaction studied (neutral, attractive) at $T=0.6$, $P=0.3$, and $N=32$ as a function of the distance $r-R_f$ from the surface of the nanoparticle. Chain end segregation to the surface is apparent for neutral interactions $R_f=2.0\sigma$, while for attractive fillers of the same size the chain end concentration is significantly smaller close to the particle. For small attractive particles, $R_f=1.0\sigma$, similar behavior to the neutral interactions for filler size $R_f=2.0\sigma$ is observed.

stant pressure. The second set of four configurations was obtained by equilibrating the ones received after the cooling process under constant volume but at a high temperature of $T=1.0$. We next prepared the minimum-energy configurations from both sets using conjugate gradient minimization. Uniaxial deformations of strain ε_{ii}, where $ii=xx$, yy or zz, were implemented by rescaling all the coordinates and the corresponding box length affinely. The energy of the system was minimized again, giving rise to the nonaffine displacement field $u(r)$. No differences were found in the resulting nonaffine displacement field for the two different methods outlined above.

III. RESULTS AND DISCUSSIONS

A. Structural analysis

The density profile of the monomers is given in Fig. 1 as a function of $r-R_f$, the distance from the surface of the particle. Distinct peaks are indicative of layering of the polymer around the particles. The local density of polymer segments, as expected, is enhanced near the surface of the particle. The attractive case (the system for which interactions between the monomers and the particle are strongly attractive) shows a clear density increase at the surface of the particle compared to the neutral case (where monomer-particle interactions are relatively weak). Our results are in agreement with literature findings for polymers near a wall [22–24] and near spherical particles [25,30,41–43]. When temperature decreases, the heights of the peaks increase for all systems, as shown previously for attractive and neutral particles [34].

Previous simulations of polymers near walls [24] and spherical particles [41] have also shown that the concentration of chain ends in the vicinity of neutral surfaces is higher than that of other monomers. Our simulations reveal a similar chain-end segregation effect. As shown in Fig. 2, for neutral interactions, the chain ends exhibit a propensity to reside near the particle surface. For attractive interactions, the larger particles ($R_f=2.0\sigma$) exhibit a concentration of chain ends near the particle surface that is significantly smaller than that observed for the same size fillers with neutral interactions. For small attractive particles however, $R_f=1.0\sigma$, a behavior similar to that observed for the neutral interactions is found. This is suggestive of a characteristic size beyond which the effects of nanoparticles start to change [44].

Polymer chains assume a distinct orientation near the particles. The second Legendre polynomial is defined as $P_2=\frac{1}{2}(3\cos^2\theta-1)$, where the angle θ is formed by the vector from the center of the nanoparticle to monomer i, and the vector between i and the next monomer on the same chain, $i+1$. The average orientation of the segments is defined by taking the ensemble average $\langle P_2\rangle$. A value of $\langle P_2\rangle=0$ indicates a random orientation $\left[\langle P_2\rangle=\int_0^{\pi}\frac{1}{2}(3\cos^2\theta-1)\sin\theta d\theta/\pi=0\right]$, while a value of -0.5 indicates perfect tangential alignment. Figure 3 shows the orientation of segments for both neutral and attractive interactions. Moving away from the surface of the particle to the bulk polymer, $\langle P_2\rangle$ decreases, reaching a minimum, and then increases to a maximum. Beyond this feature, some oscillations are observed that gradually decay to $\langle P_2\rangle=0$. For stronger polymer-particle interactions the first minimum gradually decreases. Other off-lattice simulations have also reported the tendency of segments to lie parallel to the surface for both wall [22] and spherical-particle [28,30] systems.

A measure of the affinity of monomers for packing around a particle is the "surface excess" defined as [27]

$$\Gamma_s = R^{-2}\int_R^{\infty} dr r^2 h_{pc}(r), \tag{9}$$

where $h_{pc}(r)=g_{pc}(r)-1$. A negative value of this variable indicates a tendency of the polymer to dewet the nanoparticle surface, while a positive value suggests that the polymer wets the surface of the particle. In Fig. 4 the "surface excess" is plotted for different particle sizes. For large particles the

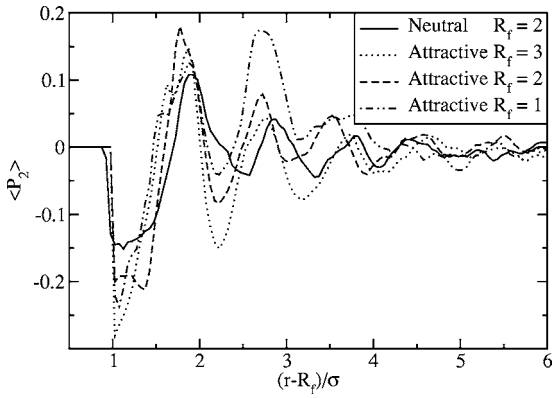

FIG. 3. Mean second Legendre polynomial P_2 between the vector from the center of the nanoparticle to the monomer i and the vector between i and the next monomer in the same chain $i+1$ at $T=0.6$, $P=0.3$ and $N=32$. $\langle P_2 \rangle$ is given as a function $r-R_f$ from the surface of the particle. The preferential alignment of the chains parallel to the surface of the particle is observed.

polymer wets the surface and Γ_s is positive [27]. When the particle size decreases the "surface excess" also decreases and for particles of $R_f=0.5$ we find that the sign of Γ_s changes. This indicates a transition from enthalpic wetting to entropic dewetting when particles become comparable to the monomer size.

B. Elastic constant calculations: single particle system

Few studies of nanocomposite systems have examined the mechanical behavior of the material. Furthermore, available reports have focused on the calculation of bulk mechanical properties, generally by applying a load or a homogeneous deformation to a sample. In contrast to previous works, the methodology employed here permits direct calculation of the local mechanical properties of the material from the spontaneous fluctuations of the stress, thereby offering unique insights into the elastic moduli of our model nanocomposites. Figure 5 shows the local shear modulus as a function of the distance from the surface of the filler for a polymer matrix containing an individual particle. The shear modulus is defined as the average $G=(C_{44}+C_{55}+C_{66})/3$ of the components of the elastic matrix. For the attractive system, the local magnitude of G increases in the vicinity of the particle surface, suggesting the existence of a "glassy" layer, even in the melt regime. This layer with enhanced mechanical properties is reminiscent of the "glassy" layer that has been invoked to interpret experimental data [3]. It has recently been shown that this layer does not homogeneously surround the nanoparticle, but that it consists of a preponderance of domains having a large positive modulus [34].

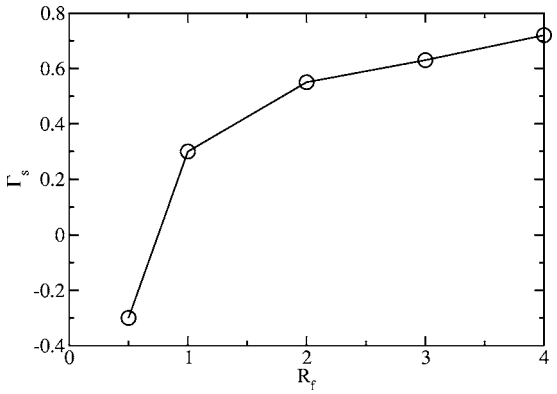

FIG. 4. Surface excess as a function of particle size at $T=0.6$, $P=0.3$, and $N=32$. A transition from enthalpic wetting ($\Gamma_s>0$) to entropic dewetting ($\Gamma_s<0$) is apparent at approximate $R_f=0.75$.

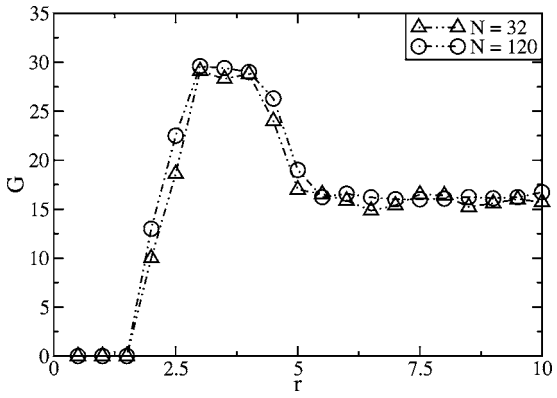

FIG. 5. Distribution of the local shear modulus with respect to the distance r from the center of the nanoparticle for attractive particles for two polymer chain lengths ($N=32,120$) at $T=0.2$ and $P=0.3$.

As mentioned earlier, the chain dimensions are altered in the vicinity of a nanoparticle, and the magnitude of such changes depends on the chain length. It is therefore of interest to consider whether chain length has an effect on the glassy layer thickness. To that end, we also performed local elastic constant calculations for a system of chains of 120 segments. As shown in Fig. 5, the glassy layer thickness does not exhibit any dependence on the polymer molecular weight. The same is true for the values of the shear modulus in the glassy layer. They remain approximately the same, regardless of chain length.

It is generally perceived that addition of nanoparticles to a polymer matrix has a more pronounced effect than addition of micron-sized particles [1]. Here we consider the effect of particle size on the mechanical properties and the thickness of the glassy layer. We find that, as the particle size decreases, the thickness and the values of the shear modulus of the glassy layer decrease [see Figs. 6(a) and 6(b)]. This trend suggests that once the particle size reaches a specific value, it no longer behaves as a constraint for the polymer chains. This behavior can be partly explained in terms of the particle surface chain-end concentration shown in Fig. 2 and its relation to the free volume. As particle size decreases, the chain end concentration increases at the particle surface, thereby generating more free volume at the surface of the particle and more space for the particles and the polymer segments to move. This larger free volume reduces the enhancement of elastic constants observed for large particles. The decrease of the glassy layer thickness can also be related to the decrease of the surface excess as shown in Fig. 4. For small particles comparable to the polymer segments the sur-

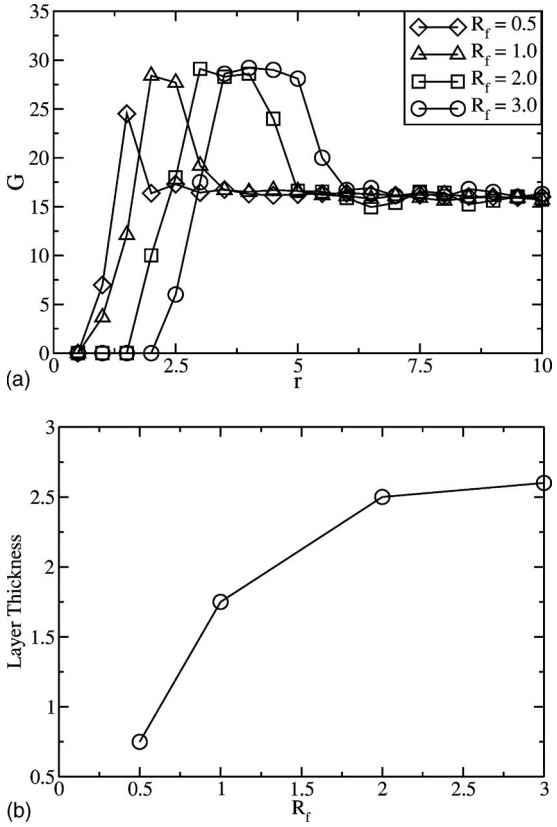

FIG. 6. (a) Distribution of the local shear modulus with respect to the distance r from the center of the nanoparticle for attractive particles of different size at $T=0.2$, $P=0.3$, and $N=32$. (b) Glassy layer thickness with respect to particle size at $T=0.2$, $P=0.3$, and $N=32$.

face excess becomes negative, thereby causing the polymer to dewet the surface and causing the glassy layer to almost disappear.

C. Elastic constant calculations: many-particle systems

Experimental evidence suggests that, as the concentration of nanoparticles increases, the observed changes of a composite's mechanical properties become more pronounced. More specifically, experimental data are often described by a simple quadratic empirical relationship [9,13] of the form

$$\frac{G^{NC}}{G^{PP}} = 1 + \frac{5}{2}\phi_p + 4.94\phi_p^2, \tag{10}$$

where G^{NC} is the shear modulus of the composite, G^{PP} is the shear modulus of the unfilled (pure) polymer matrix and ϕ_p is the volume fraction of the particles. A similar expression exists [9,13] for the Young's modulus,

$$E = \frac{\bar{C}_{44}(3\bar{C}_{12} + 2\bar{C}_{44})}{\bar{C}_{12} + \bar{C}_{44}}, \tag{11}$$

where $\overline{C_{12}}=(C_{12}+C_{13}+C_{23})/3$ and $\overline{C_{44}}=(C_{44}+C_{55}+C_{66})/3$,

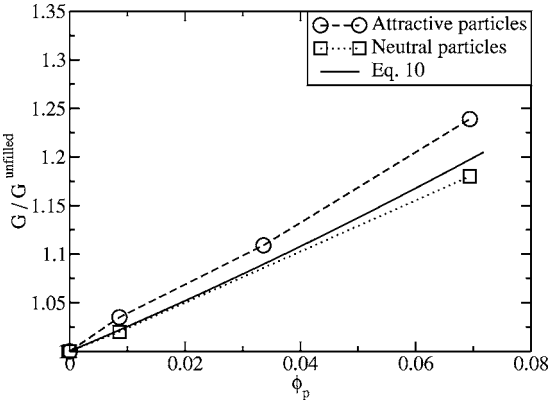

FIG. 7. Effect of volume fraction of nanoparticles of $R_f=2.0\sigma$ on shear modulus at $T=0.2$, $P=0.3$, and $N=32$.

$$\frac{E^{NC}}{E^{PP}} = 1 + \tfrac{5}{2}\phi_p + 14.1\phi_p^2. \tag{12}$$

Figure 7 confirms that Eq. (10) describes qualitatively our data. However, as it does not include any dependence on

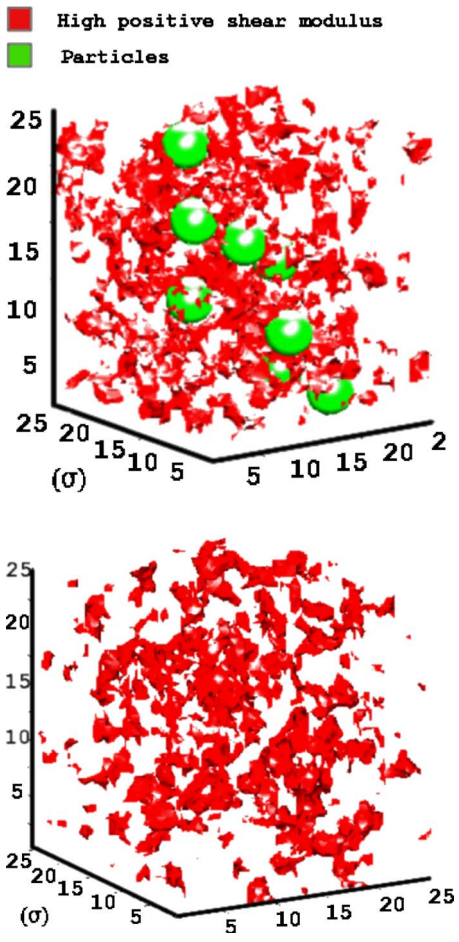

FIG. 8. (Color online) 3D distribution of domains of high positive shear modulus for the nanocomposite of particles of size $R_f=2.0\sigma$ and the pure polymer glasses at $T=0.2$, $P=0.3$, $\phi\sim0.07$, and $N=32$.

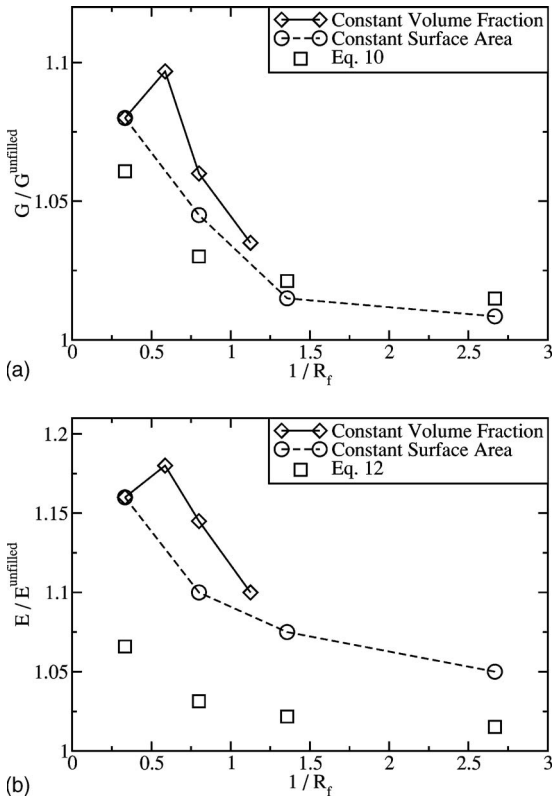

FIG. 9. Investigation of the effect of surface area and volume fraction of the nanoparticles on the (a) shear modulus and (b) Young's modulus of nanocomposites. The squares represent constant surface area results using Eqs. (10) and (12) for the calculation of G and E for each particle size. (Constant volume fraction $\phi=0.024$ and constant surface area $a=0.011\sigma^{-1}$ at $T=0.2$, $P=0.3$, and $N=32$.)

particle size or interfacial properties, Eq. (10) does not reproduce the observed differences between attractive and neutral particles.

The nonlinearity of the relationship between volume fraction and elastic moduli suggests that a simple mixing rule (e.g., an average of the glassy layer mechanical properties and those of the pure polymer) is insufficient to describe the behavior of the composite systems considered in this work. A color map of the local shear modulus of the pure polymer glass and the nanocomposite for the system of attractive particles is presented in Fig. 8. The elastic moduli of polymeric glasses are inhomogeneous, as shown in previous work [34,39]. For the unfilled polymer, domains of high modulus are distributed uniformly throughout the system. In the nanocomposite material, the population of high-modulus domains is higher near the particles. Furthermore, particles that are close to each other give rise to the formation of regions of high modulus that span or bridge the entire space between them.

In order to investigate this behavior further we also performed molecular dynamics calculations in the NVE ensemble. The velocities of the particles and segments were at first initialized at a temperature $T=0.00\,001$, and the systems were equilibrated for 50 000 steps. The equilibration period was followed by a production run of 200 000 steps with

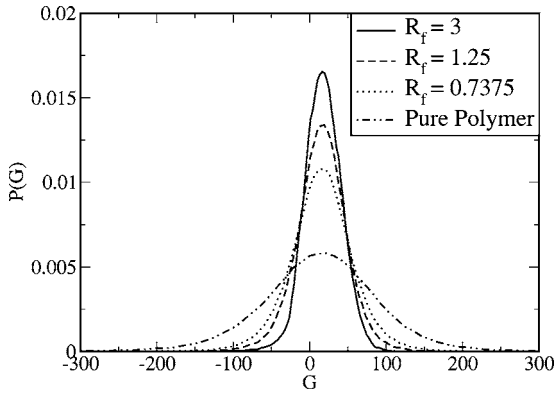

FIG. 10. Effect of particle size on the distribution of the local shear modulus G with respect to particle size keeping the volume fraction constant ($\phi=0.023$) at $T=0.2$, $P=0.3$, and $N=32$.

timestep $\Delta t=0.001$. The particle and segment positions were sampled every 100 steps. The average displacement from the center of mass of the particles and the segments can be related experimentally to the Debye-Waller factor [45]. The average displacement of the polymer segments of the nanocomposite $\langle\sqrt{r_{NC}^2}\rangle=0.001\,22$ was found to be smaller than for the pure polymer $\langle\sqrt{r_{PP}^2}\rangle=0.001\,28$, consistent with the higher values of moduli of the nanocomposite compared to the pure polymer. For the nanocomposite, we calculate the local average displacement of segments in a shell of 2.0σ surrounding the nanoparticle and also in a cylinder of 2.5σ diameter between nanoparticles that are closer than 9σ. We find that the displacement in the shell $\langle\sqrt{r_{NC\ \mathrm{shell}}^2}\rangle=0.000\,92$ is significantly smaller than in the bulk of the material, in agreement with our previous findings of glassy-layer formation around the particle. The region of the cylinder between the particles appears to also exhibit smaller displacements, $\langle\sqrt{r_{NC\ \mathrm{cylinder}}^2}\rangle=0.001\,04$, which can be related to the higher population of high-moduli domains between the particles that appear as bridges in Fig. 8.

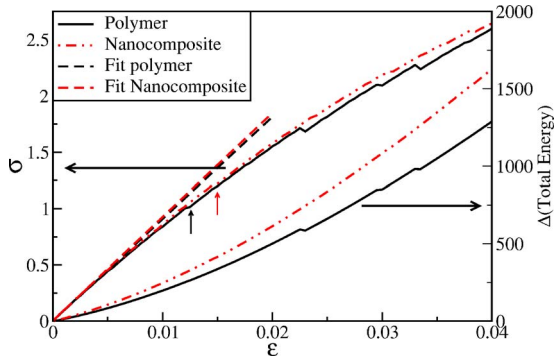

FIG. 11. (Color online) Stress strain curve for both pure polymer and nanocomposite system with a strain rate of 5×10^{-4}/step. The nanocomposite curve is at all times higher than the pure polymer indicating a stronger material. The plastic events (drops in the stress) occur for the nanocomposite in higher strains than pure for the unfilled polymer suggesting a tougher material. The difference in total energy is plotted with respect to the strain. It is clear that the energy strain curve is not as sensitive to the plastic events.

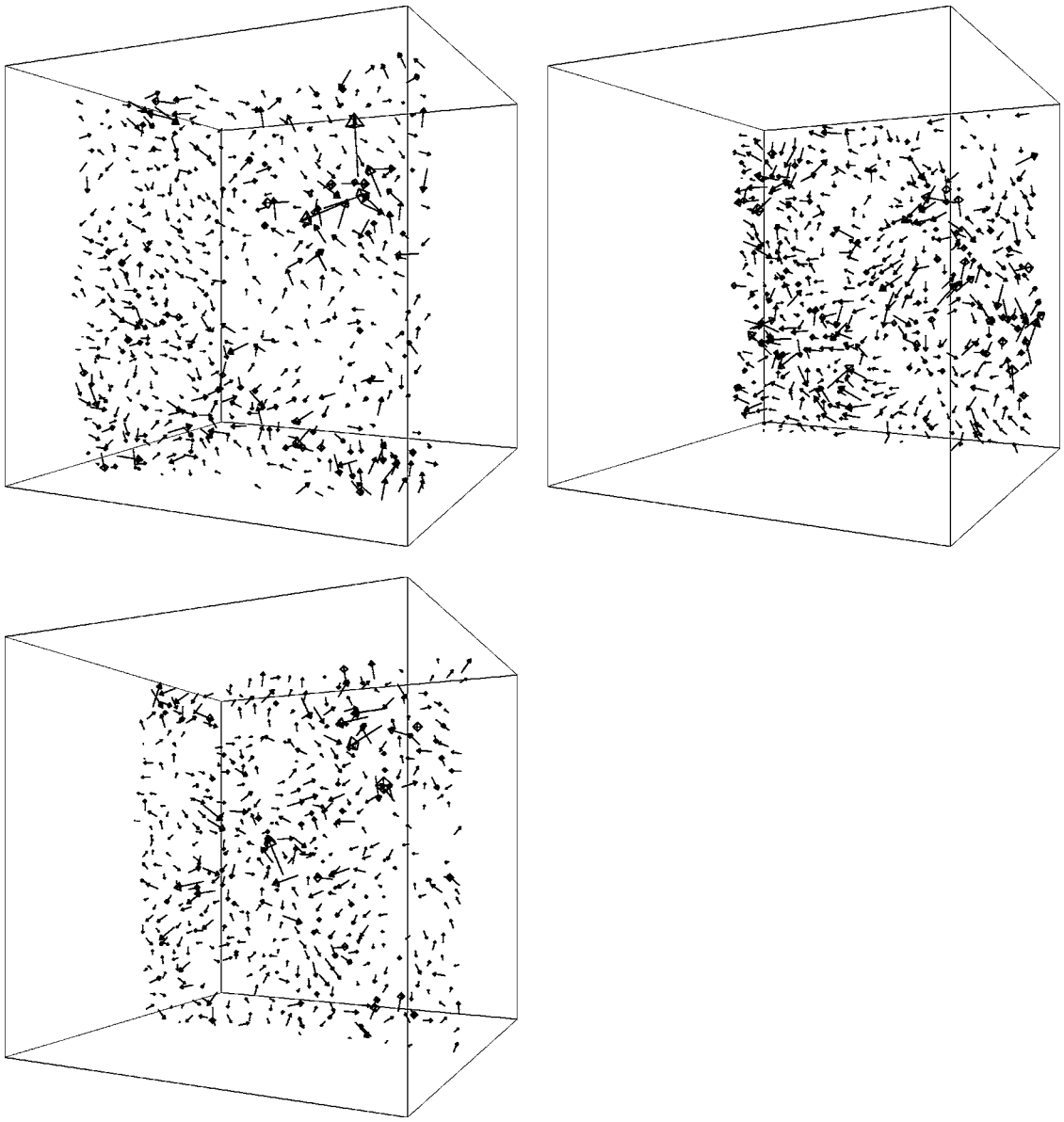

FIG. 12. Typical snapshots of the nonaffine displacement field $u(r)$ for the unfilled polymer in layers of thickness 1σ obtained after applying a uniaxial deformation of strain 10^{-5}.

We now address the significance of particle size for nanocomposite behavior, which is directly related to the importance of interface effects [1,4,8]. For small particles, the volume fraction is not sufficient to quantify the mechanical properties of nanocomposites, and the surface area per unit volume becomes another relevant variable. We performed calculations in which the number of nanoparticles and their size were varied in a systematic manner in order to quantify the relative importance of volume fraction and surface area. One parameter, surface area or volume fraction, is kept constant while the other changes. We characterize the elasticity of the system through the shear modulus, G and the Young's modulus, E.

The number of particles and particle diameter were modified in such a way as to keep constant the volume fraction (ϕ=0.024) or the surface area per unit volume, $a=0.011\sigma^{-1}$. At constant volume fraction, it is clear that decreasing the particle size (hence increasing the surface area) results initially in an increase of G and E, as can be seen in Fig. 9. However, once the particles become sufficiently small, both shear and Young's modulus start to decrease. These results suggest that particles cease to act as topological constraints when their size becomes comparable to that of the monomer. This cessation of constraining can be related to an increase in the "mobility" of the particles, which is connected to the free volume via the chain end concentration (see Fig. 2) and to the decrease of surface excess (see Fig. 4). Evidence for the existence of such a characteristic length was also provided by the experiments of Roberts *et al.* [10], where even more dramatic changes on the mechanical properties were reported. Larger particles were found to behave as reinforcing agents, while smaller particles as plasticizers. In our systems, the particle-polymer interaction is strong and we do not observe such a pronounced decrease of the me-

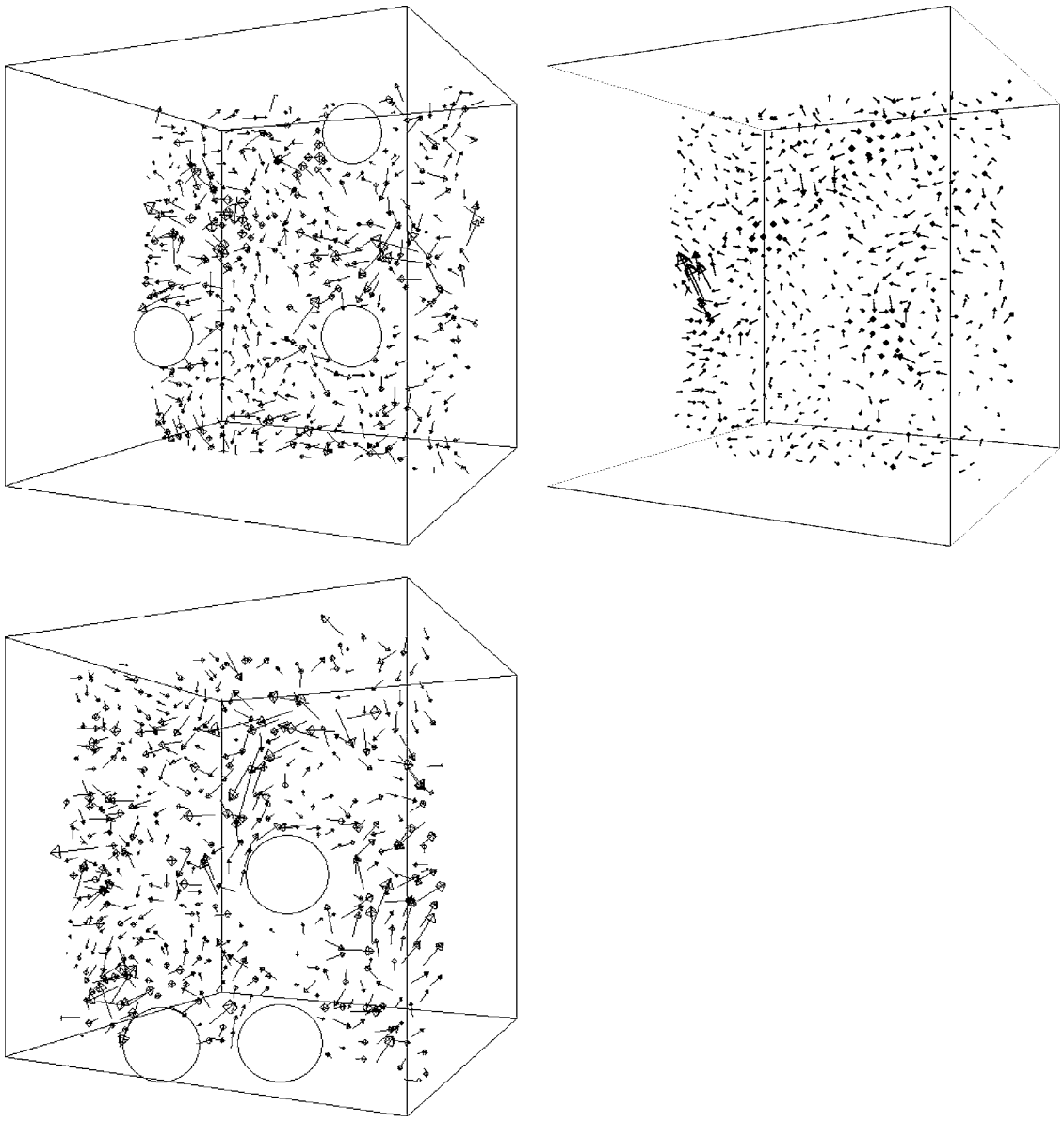

FIG. 13. Typical snapshots of the nonaffine displacement field $u(r)$ for the nanocomposite system of volume fraction $\phi \sim 0.07$ and particle size $R_f = 2\sigma$ in layers of thickness 1σ obtained after applying a uniaxial deformation of strain 10^{-5}.

chanical properties. The filled polymer exhibits higher elastic moduli than the unfilled polymer for any volume fraction or surface area, and there is no evidence of plastification.

At constant surface area, increasing the number of particles causes the volume fraction to decrease. The modulus decreases monotonically. The simulation results for the Young's modulus are always higher than the ones predicted from the empirical relationship [see Fig. 9(b)]. For the shear modulus a crossover exists, and at high particle size the empirical relationship underpredicts the simulation results while for extremely small particles it overpredicts them [see Fig. 9(a)].

We also examined the distribution of the local shear modulus for the constant particle volume fraction systems. As shown earlier, the nanocomposite is found initially to exhibit higher values of shear and Young's modulus when the particle radius is decreased and the surface area is increased, followed by a decrease of the values of the moduli below a characteristic particle size. At the same time, for a given level of resolution, the distribution of local shear modulus becomes broader when the particle size is increased, as seen in Fig. 10. This suggests that, for constant particle volume fraction, regardless of the reinforcement of the material, the level of mechanical inhomogeneity is increased by decreasing particle size.

D. Nonaffine displacement field

We perform calculations similar to those used by Malandro *et al.* [46] for a glass model. We apply a uniaxial deformation to both systems in steps of strain 5×10^{-4} and after each affine deformation, we minimize their energy while keeping the shape and volume constant. We calculate the stress for each of these steps; a stress strain curve is obtained

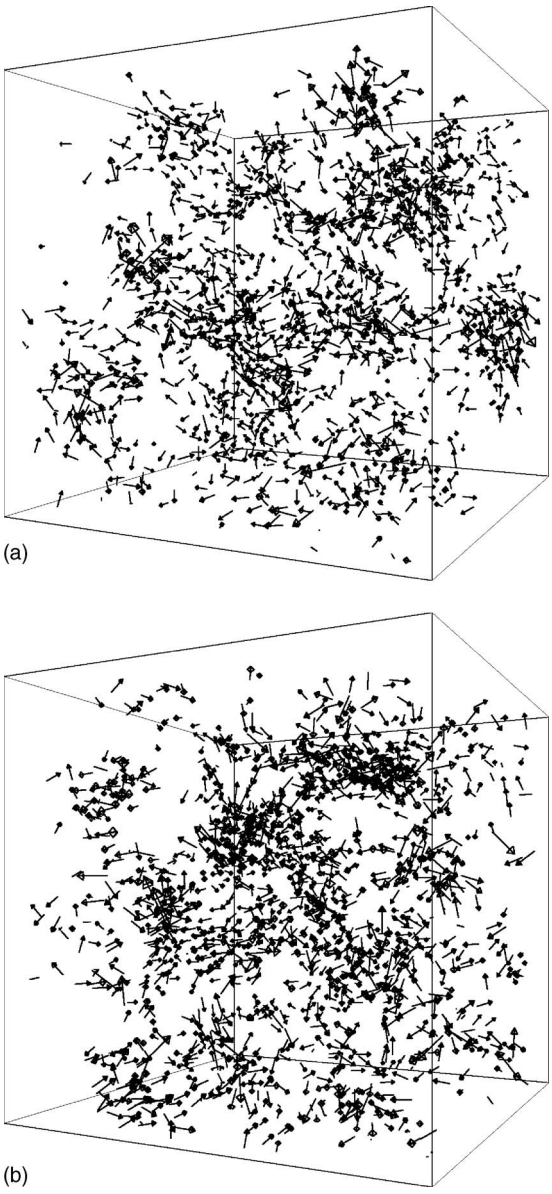

FIG. 14. (a) 3D plot of the 10% higher nonaffine displacements for the unfilled polymer. (b) 3D plot of the 10% higher nonaffine displacements for the nanocomposite. Nonaffine displacements obtained for a uniaxial deformation of strain 10^{-5}.

and plotted in Fig. 11. The curve for the nanocomposite is at all times higher than that for the pure polymer, indicating a stronger material. The sudden drops of stress that appear in the stress strain curve have been related in the literature [46] to plastic events. These plastic events occur for the nanocomposite at higher strains than for the pure polymer and are more rare. This result suggests that the nanocomposite is not only a stronger material but also tougher. The difference in total energy is plotted for both systems with respect to the strain. It is clear that the energy strain curve does not capture all the plastic events.

We now turn our attention to the analysis of deformation of the material. The nonaffine displacements are determined according to the procedures outlined in the Methodology section. Typical realizations of such fields for a strain value

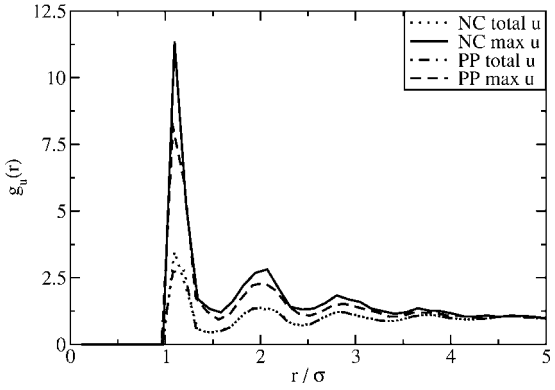

FIG. 15. Pair distribution of the nonaffine displacements. We refer as max to the 10% highest non-affine displacements. From the distribution of the highest nonaffine displacements it is clear that these displacements exhibit a propensity to occur near each other forming clusters of nonaffinely displaced segments. For the nanocomposite system this effect is more pronounced. Nonaffine displacements obtained for a uniaxial deformation of strain 10^{-5}.

of 10^{-5} are presented in Figs. 12 and 13, where cross sections (slabs) of configurations are shown for both systems (pure polymer and nanocomposite). In Figs. 14(a) and 14(b) we plot only the higher 10% nonaffine displacements. A simple visual inspection of these fields reveals that the higher nonaffine displacements tend to form clusters. Figure 15 shows the pair distribution corresponding to these displacements; which also shows that these displacements exhibit a propensity to occur near each other, giving rise to the formation of "clusters" of nonaffinely displaced segments. This effect is more pronounced for the nanocomposite system.

The participation ratio for the nonaffine displacements [33], defined by

$$P_r = \frac{1}{N}\frac{\left(\sum_i u_i^2\right)^2}{\sum_i (u_i^2)^2}, \tag{13}$$

where i is the particle index and N the number of particles and segments, can be used to measure the critical strain where the transition from elastic to plastic regime occurs. Large values of participation ratio indicate that elastic nonaffine displacements involve a substantial fraction of the particles. When the deformation exceeds the plastic threshold, P_r falls rapidly, indicating that a plastic deformation proceeds via highly localized events. It is clear from Fig. 16 that both systems exhibit a similar behavior. However, at all times, the curve corresponding to the nanocomposite system exceeds that of the pure polymer. By comparing the participation ratio curves for the two systems it becomes apparent that the critical strain for the nanocomposite system is larger than that of the pure polymer. This finding suggests that inclusion of nanoparticles creates a material (nanocomposite) less susceptible to failure than the pure polymer. The elastic character of these deformations was verified by imposing a reverse deformation that compresses the system back to its initial shape. The residual field indicated by $\langle \|v\| \rangle$ was calculated; for a completely reversible deformation $\langle \|v\| \rangle$ should

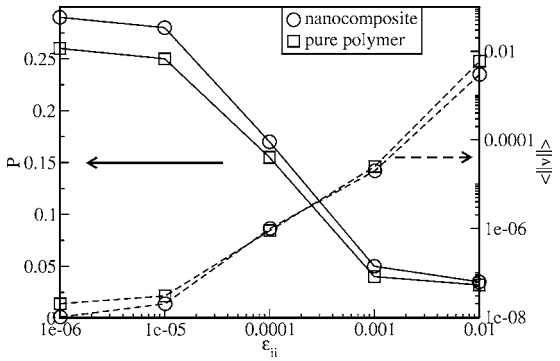

FIG. 16. Participation ratio P_r as a function of applied strain (solid lines) and residual plastic displacement field $\langle\|v\|\rangle$ (dashed lines) obtained by reverse transformation back to the original macroscopic shape. Residual fields below 10^{-8} are due to numerical inaccuracies and the field is considered as reversible. For the nanocomposite system the particle volume fraction is $\phi \sim 0.07$ and particle size $R_f = 2\sigma$.

be zero. It is clear from the results in Fig. 16 that the residual field is negligible below the critical strain, thereby emphasizing that these deformations (of strain below the critical) are elastic and reversible.

To further analyze the nature of nonaffine displacements, we focus on a strain of $\varepsilon = 10^{-5}$, for which the participation ratio for both the systems is relatively high but the systems are still in the elastic regime [33]. For this strain value, the correlation of the nonaffine field is analyzed by calculating the function

$$C(r) = \frac{\langle u(r)u(0)\rangle}{\langle u(0)^2\rangle} \tag{14}$$

for all segments separated by a distance r. This correlation function is shown in Fig. 17; it is related to the fragility and

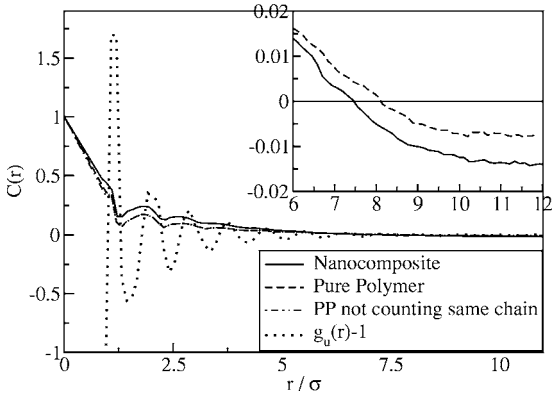

FIG. 17. Correlation function $C(r)$ of the nonaffine displacement field as a function between pairs of distance r for the unfilled polymer and the nanocomposite system of volume fraction $\phi \sim 0.07$ and particle size $R_f = 2\sigma$. For comparison of the peaks of the correlation functions, the polymer segment pair distribution function $g(r)$ is plotted and the polymer correlation function not counting contributions between nonaffine displacements of segments belonging in the same chain. Inset: Magnification of long-range results.

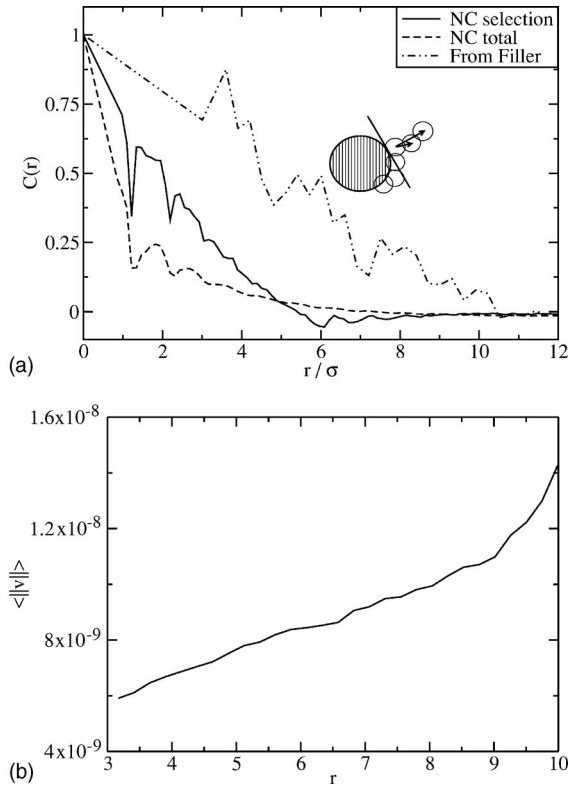

FIG. 18. (a) Correlation function $C(r)$ of the nonaffine displacements as a function between pairs of distance r starting from polymer beads lying in a shell of thickness 1.5σ around the particle with the rest of the system on the opposite side of the particle separated by an imaginary surface passing as shown in the figure. Also the correlation starting from the filler is plotted and for comparison the total nanocomposite correlation function counting all contributions is given. Nonaffine displacements obtained for a uniaxial deformation of strain 10^{-5}. (b) Distribution of magnitude of residual plastic displacements around a nanoparticle. Residual plastic displacements obtained from reverse deformation that compresses the systems back to their initial shape upon a uniaxial deformation of strain 10^{-5}.

mechanical stability of a material. Several interesting features are detected. First, we note that the correlation length, ξ, for the polymeric systems considered in this work is significantly smaller than that observed in the Lennard-Jones binary glasses considered by Leonforte *et al.* [33]. Second, we find that the correlation length corresponding to the nanocomposite system is smaller ($\xi_{NC}=7.5$) than that of the pure polymer ($\xi_{PP}=8.0$), suggesting that the system is more mechanically homogeneous and stable [47]. This is consistent with the narrower distribution of local shear moduli observed for the nanocomposite systems. Leonforte *et al.* [33] found that for a binary glass, the frequency of the boson peak is correlated with $\omega = c_T 2\pi/\xi$, where c_T is the transverse velocity of sound, equal to $c_T = \sqrt{G/\rho}$, where G as mentioned earlier is the shear modulus and ρ is the density. Using this relation one can calculate an estimate for the value of the frequency of the boson peak for the two systems, and obtain a measure of the material's fragility [48]. The transverse velocity of sound c_T has a value of 4.30 for the nanocomposite system, while for the pure polymer it is 3.84. From these

data and the results for the correlation length (ξ_{NC}=7.5 and ξ_{PP}=8.0), we find that the frequency of the boson peak is ω_{NC}=3.6 for the nanocomposite and, for the pure polymer, it is ω_{PP}=3.0. As shown by Chumakov *et al.* [48], these values for the boson peaks imply that the nanocomposite is less fragile than the polymer. Novikov *et al.* [49] have correlated the fragility of materials to their mechanical properties, particularly the ratio of the bulk to the shear modulus K/G. The higher this ratio, the more fragile the material is. For the two systems considered in this section, we estimate $(K/G)_{NC}$=3.15 and $(K/G)_{PP}$=3.45. Again we arrive at the same conclusion, namely the fact that the nanocomposite system is stiffer (has higher elastic moduli), less fragile, and less anharmonic (in the "Angell" sense) than the pure polymer [50–52].

We conclude our investigation of nanocomposites with a calculation of two correlation functions: one from the filler with the rest of the system, and a second one from a shell of polymer beads around the filler with the rest of the system. The shell thickness is chosen to be 1.5σ. As shown in Fig. 18(a), a polymer segment in the shell is chosen and its correlation with part of the system is calculated. This procedure ensures that the nanoparticle that is surrounded by this shell is not included in the analysis. The chosen part is the one on the opposite side of the particle separated by an imaginary plane tangent to the particle surface. It is found that the filler-polymer correlation length is higher than that of the pure polymer, while the glassy layer-polymer selection correlation length is smaller than the one of the nanocomposite system. This suggests that the layer surrounding the particles is more mechanical homogeneous than the rest of the polymer. To justify this analysis we also calculated the distribution of the magnitude of residual plastic displacements around a nanoparticle. The residual plastic displacements were obtained from reverse deformations that compress the system back to its initial shape after a uniaxial deformation of strain $\varepsilon 10^{-5}$. As seen in Fig. 18(b), close to the particles the magnitude of the residual displacements appears to be smaller than away from it. This verifies that the material closer to the particles is more mechanically homogeneous than the rest of the polymer.

IV. CONCLUSIONS

With the aid of MC simulations changes of mechanical properties when nanoparticles are being added to the polymer matrix were explored. By varying the polymer-nanoparticle interaction we were able to arrive to conclusions necessary for the design of nanocomposite systems with desired mechanical properties. Attractive nanoparticles were found to increase the Young's modulus compared to the unfilled polymer. An increase of the local $\overline{C_{44}}$ at the vicinity of the particle is indicative of a glassy layer. The effect of particle size and chain length on the glassy layer and that of surface area and volume fraction were investigated. When the particle size reaches a certain value the particles cease being topological constraints. Finally from the calculation of the nonaffine displacement field a useful insight was obtained. The fragility of the nanocomposite glass is lower than the unfilled polymer. Despite the simplicity of the model our results qualitatively give a clear view of changes induced by nanoparticle addition in a polymer matrix.

Our findings in this work are closely related to the so-called interaction zone theory. An alternative theory for the origin of increased strength is the bridge theory, which involves the particle chain network formation. When the particle-to-particle distance is small or comparable to less than two radius of gyration radii then a chain can wrap around a particle and at the same time wrap around another creating a network that as is proposed from the bridge formation theory will increase the mechanical properties of the matrix. Ongoing work involves simulation of polymers with different chain lengths and many nanoparticle composite systems so that the bridge formation theory can be investigated.

ACKNOWLEDGMENTS

This work was supported by the NSF (NIRT Grant No. CTS-0506840). Partial support from the Semiconductor Research Corporation (SRC) is gratefully acknowledged. Valuable discussions with R. Riggleman and A. Tanguy are appreciated.

[1] P. Vollenberg and D. Heikens, Polymer **30**, 1656 (1989).
[2] Y. Ou, F. Yang, and Z. Yu, J. Polym. Sci., Part B: Polym. Phys. **36**, 789 (1998).
[3] J. Berriot, H. Montes, F. Lequeux, D. Long, and P. Sotta, Macromolecules **35**, 9756 (2002).
[4] B. Ash, R. Siegel, and L. Schandler, Macromolecules **37**, 1358 (2004).
[5] R. A. Narayanan, P. Thiyagarajan, S. Lewis, A. Bansal, L. Schadler, and L. B. Lurio, Phys. Rev. Lett. **97**, 075505 (2006).
[6] G. Tsagaropoulos and A. Eisenberg, Macromolecules **28**, 396 (1995).
[7] J. Berriot, F. Lequeux, L. Monnerie, H. Montes, D. Long, and P. Sotta, J. Non-Cryst. Solids **307**, 719 (2002).
[8] S. Vieweg, R. Unger, G. Heinrich, and E. Donth, J. Appl. Polym. Sci. **73**, 495 (1998).
[9] R. Chahal and L. S. Pierre, Macromolecules **2**, 193 (1969).
[10] C. Roberts, T. Cosgrove, R. Schmidt, and G. Gordon, Macromolecules **34**, 538 (2001).
[11] E. Kopesky, T. Haddad, G. McKinley, and R. Cohen, Polymer **46**, 4743 (2005).
[12] M. MacKay, T. Dao, A. Tuteja, D. Ho, B. V. Horn, H. Him, and C. Hawker, Nat. Mater. **2**, 762 (2003).
[13] G. Smith, D. Bedrov, L. Li, and O. Byutner, J. Chem. Phys. **117**, 9478 (2002).
[14] D. Hull and T. Clyne, *An Introduction to Composite Materials*, 2nd ed. (Cambridge University Press, Cambridge, 1996).
[15] T. Mura, *Micromechanics of Defects in Solids*, 2nd ed. (Martinus Nijhoff Publishers, 1987).

[16] J. Halpin and J. Kardos, Polym. Eng. Sci. **16**, 344 (1976).
[17] T. Mori and K. Tanaka, Acta Metall. **21**, 571 (1973).
[18] T. Fornes and D. Paul, Polymer **44**, 4993 (2003).
[19] E. Kopesky, T. Haddad, R. Cohen, and G. McKinley, Macromolecules **37**, 8992 (2004).
[20] M. Osman, A. Atallah, G. Kahr, and U. Suter, J. Appl. Polym. Sci. **83**, 2175 (2002).
[21] H. Lusti, I. Karmilov, and A. Gusev, Soft Mater. **1**, 115 (2003).
[22] C. Abrams and K. Kremer, J. Chem. Phys. **115**, 2776 (2001).
[23] T. Aoyagi, J. Takimoto, and M. Doi, J. Chem. Phys. **115**, 552 (2001).
[24] I. Bitsanis and G. Hadziioannou, J. Chem. Phys. **92**, 3827 (1990).
[25] M. Vacatello, Macromolecules **34**, 1946 (2001).
[26] T. Desai, P. Keblinski, and S. Kumar, J. Chem. Phys. **122**, 134910 (2005).
[27] J. Hooper, K. Schweizer, T. Desai, R. Koshy, and P. Keblinski, J. Chem. Phys. **121**, 6986 (2004).
[28] M. Doxastakis, Y.-L. Chen, O. Guzmán, and J. de Pablo, J. Chem. Phys. **120**, 9335 (2004).
[29] A. Nakatani, W. Chen, R. Schmidt, G. Gordon, and C. Han, Polymer **42**, 3713 (2001).
[30] D. Brown, P. Mélé, S. Marceau, and N. Alberola, Macromolecules **36**, 1395 (2003).
[31] M. Sharaf and J. Mark, Polymer **45**, 3943 (2004).
[32] T. Bohme and J. de Pablo, J. Chem. Phys. **116**, 9939 (2002).
[33] F. Leonforte, R. Boissière, A. Tanguy, J. Wittmer, and J.-L. Barrat, Phys. Rev. B **72**, 224206 (2005).
[34] G. J. Papakonstantopoulos, K. Yoshimoto, M. Doxastakis, P. F. Nealey, and J. J. de Pablo, Phys. Rev. E **72**, 031801 (2005).
[35] J. de Pablo, M. Laso, and U. Suter, J. Chem. Phys. **96**, 2395 (1992).
[36] Z. Chen and F. Escobedo, J. Chem. Phys. **113**, 11382 (2000).
[37] B. Banaszak and J. de Pablo, J. Chem. Phys. **119**, 2456 (2003).
[38] N. Karayiannis, V. Mavrantzas, and D. Theodorou, Phys. Rev. Lett. **88**, 105503 (2002).
[39] K. Yoshimoto, T. S. Jain, K. Van Workum, P. F. Nealey, and J. J. de Pablo, Phys. Rev. Lett. **93**, 175501 (2004).
[40] J. Lutsko, J. Appl. Phys. **64**, 1152 (1988).
[41] R. Picu and M. Ozmusul, J. Chem. Phys. **118**, 11239 (2003).
[42] F. Starr, T. Schrøder, and S. Glotzer, Macromolecules **35**, 4481 (2002).
[43] P. Scheidler, W. Kob, and K. Binder, Europhys. Lett. **59**, 701 (2002).
[44] R. Riggleman, K. Yoshimoto, J. Douglas, and J. de Pablo, Phys. Rev. Lett. **97**, 045502 (2006).
[45] R. Hempelmann, *Quasielastic Neutron Scattering and Solid State Diffusion*, 1st ed. (Oxford Science, Oxford, 2000).
[46] D. Malandro and D. Lacks, J. Chem. Phys. **110**, 4593 (1999).
[47] L. E. Silbert, A. J. Liu, and S. K. Nagel, Phys. Rev. Lett. **95**, 098301 (2005).
[48] A. I. Chumakov, I. Sergueev, U. van Burck, W. Schirmacher, T. Asthalter, R. Ruffer, O. Leupold, and W. Petry, Phys. Rev. Lett. **92**, 245508 (2005).
[49] V. Novikov and A. Sokolov, Nature (London) **431**, 961 (2004).
[50] P. Bordat, F. Affouard, M. Descamps, and K. L. Ngai, Phys. Rev. Lett. **93**, 105502 (2004).
[51] C. Angell, "Strong and fragile liquids," in *Relaxation in Complex Systems*, 1st ed. (US Dept. of Commerce, Springfield, 1985).
[52] L. Martinez and C. Angell, Nature (London) **410**, 663 (2001).